processes

MDPI

Article

Experimental Study on Compression Deformation and Permeability Characteristics of Grading Broken Gangue under Stress

Yu Zhang [1], Wei Zhou [2,*], Ming Li [1,*] and Zhanqing Chen [1]

[1] State Key Laboratory for Geomechanics and Deep Underground Engineering, China University of Mining and Technology, Xuzhou 221116, China; zhangyucumt1981@126.com (Y.Z.); chenzhanqing@vip.163.com (Z.C.)

[2] College of Mining Engineering, China University of Mining and Technology, Xuzhou 221116, China

* Correspondence: loutian1982@126.com (W.Z.); mingl@cumt.edu.cn (M.L.); Tel.: +86-138-1531-4985 (W.Z.); +86-135-8547-7939 (M.L.)

Received: 16 October 2018; Accepted: 4 December 2018; Published: 9 December 2018

Abstract: As the important raw material for backfill mining, broken gangue's deformation and permeability characteristics directly affect the deformation of the overlying strata above the filling space. In this paper, through lateral compression and pressed seepage tests, the deformation and permeability characteristics of broken gangue as a function of the stress level and grading features were studied. This research indicates that the stress of broken gangue increases exponentially with an increase in strain, and the compression modulus and compression rate present a positive correlation. The samples with discontinuous grading are more difficult to compress than the continuous grading samples, and the discontinuous grading samples are tighter in accordance with the increase in compression rate. At the same time, the change range of the seepage velocity and permeability of the broken gangue decreases. Positive correction between the grading index of the broken gangue and the effect of reducing the permeability of samples is more obvious under axial compression, and less axial stress is needed to achieve the same permeability level for discontinuous grading. This paper can provide an important test basis for the design of grading parameters and the prediction of filling effects of broken gangue on backfill mining.

Keywords: permeability characteristics; grading broken gangue; compressive stress; compression deformation

1. Introduction

Many high fragmentation and porous particle structures from broken rock mass are produced during geological movement, such as fault fractured zones [1–3] and the fillings of collapse columns [4–6]. In mine construction, large amounts of broken rock mass are required, such as for gangue filling mining backfill [7,8], tailing dam construction [9], and reinforcement technology for rock roadways [10,11]. Broken rock mass still has a certain residual bearing capacity, and its deformation and seepage behaviours have a great influence on the internal fluid and gas migration. Therefore, it is of significant importance to study the deformation and permeability of broken rock mass for safety and green mining.

The deformation characteristics of broken rock mass are basic mechanical properties that greatly impact the research of controlling surface subsidence by filling mining [12,13], building tunnels and roadways passing through a fault fracture zone [14], and fixing foundations and subgrades [15]. Dong et al. (2015) studied the influence of mass density, moisture content and confining pressure on the deformation of broken rock mass [16]. The results of this research not only gave the characteristics of stress-strain relationship that show hardening at first and then softening, but also indicated that the

properties of broken sandstone under low confining pressure are characterized by shear contraction and that the high confining pressure will result in shear dilation. In addition, broken gangue has a high sensitivity to the rate of water content. Yin et al. (2012) analysed the plastic deformation and stability of rock mass under dynamic loads, and studied the reasonable critical failure strain which showed that the critical stress increased in proportion to confining pressure [17]. In other words, the critical stress and confining pressure have a positive correlation.

The permeability of broken rock mass has great significance to the safe and efficient production of mines, especially to water-conductive fault zone [18], water prevention and control of the surrounding rock of collapse columns [19,20], and in situ solution mining and migration of mining pollutants [21]. Many scholars have made great achievements in studying the penetrating characteristics of broken rock mass by testing. Chai et al. (2002) provided the mechanism of water bursting caused by deformation and failure according to the nonlinear seepage characteristics of broken rock mass [22]. Using a pressure permeability test, Min et al. (2004) found that the permeating properties of broken rock mass change greatly with the displacement of the load [23]. Through these experiments, the relations of the pore pressure gradient and the seepage velocity of the broken rock mass were obtained. Finally, the results indicated the existence of nonlinear seepage characteristics. However, due to the limitation of experimental equipment and technology, there have been few studies on the relationship between the deformation under loads and permeability of broken rock mass. Some scholars regarded the change in porosity as a deformable characteristic of broken rock mass and established the relationship between the porosity and permeability [24–26]. The basic reason for the deformation of broken rock mass is the change in the stress state, but the relationship between permeability and bearing stress changes is unclear. In addition, the particle size is the basic property of broken rock mass, this property has a great impact on stocking states, pore structure, and deformation under loads. The above broken rock mass are the ideal single particle size or a simple proportion of mixed sample. However, some relevant studies had shown that the mixed particles with a certain size grading characteristic can be piled up into a tight state. Therefore, the grading features have a certain effect on the deformation and permeability [27,28].

The research object selected in this paper is broken gangue, a by-product of coal mining. The deformation and permeability characteristics of broken gangue were analysed through experimental results by confined compression and pressure seepage tests, and evaluate the influence of stress and grading on compressibility and permeability of broken rock mass. The results can provide an important basis for the technology of gangue filling mining.

2. Test System and Sample Preparation

2.1. Test Samples

In this experiment, coal gangue (Zhangji Colliery, Huainan, China) is used as the test target. Coal gangue is the waste produced by coal mining and processing, which is the raw material for backfill mining. The bulk gangue is initially broken into small pieces in the crusher (Zhengzhou Hengxing Heavy Equipment Co., Ltd., Zhengzhou, China); then, the broken gangue particles with different particle sizes are obtained by using a crusher and grading sifter (Gaofu Machinery Co., Ltd., Xinxiang, China). The apertures of the sifter are 5, 10, 15, 20, and 25 mm, and by using the sifter, a single particle size between the ranges of 0–5, 5–10, 10–15, 15–20, and 20–25 mm were obtained, respectively, as shown in Figure 1.

Figure 1. Different particle sizes of gangue and a grading sifter.

The samples used in the experiment were obtained by mixing the single-grain gangue particles in certain proportions. According to the particle interference theory of G. A. Wegmouth [29], in order to achieve the densest state after mixing particles of different sizes, the pores between large-sized particles should be filled by smaller-sized particles, and the particle size of the filler particles cannot be larger than the gap between the large particles. The present grading method designs are the continuous grading method and the discontinuous grading method; the difference between the methods is that the particle sizes determined by the continuous grading method are consecutive, whereas some particles would be lost by the other method.

According to the theory of Talbot Grading [30], the proportion of particle diameter gangue in continuous grading samples could be described by Equation (1):

$$P_i = \left(\frac{d_i}{d_{\max}}\right)^n \tag{1}$$

where P_i is the proportion of the particle size of d_i, $d_{\max}$ is the largest diameter particle in the mixed sample (mm), and n is the power exponent of Talbot.

The n of the Talbot power exponent can be equal to 0.1, 0.3, 0.5, 0.7, and 0.9, and the maximum particle size $d_{\max}$ is 25 mm. According to Equation (1), the proportion of particles d_i can be calculated for different continuous grading samples. Since some particle sizes are lost in the samples by discontinuous grading, discontinuous grading samples can be obtained by rejecting the first-order particle size by continuous grading. The maximum and minimum sizes are required to retain in mixed-grade samples, which are framework grain and pore-filled particles, respectively. Samples with the sizes of 5–10, 10–15, and 15–20 mm are removed in the continuous grading, which correspond to the index m with 0.3, 0.5 and 0.7 mm, respectively. The removed particles will be supplemented by smaller samples with original proportions. The particle sizes of continuous-grade and discontinuous-grade samples is shown in Table 1. Where n is continuous grading index, m is discontinuous grading index, d_i is the particle size, and P_i is the proportion of the particle size of d_i.

Table 1. Proportion of particles in different grading index samples.

Grading Index		P_i(%)				
		d_1 (0–5 mm)	d_2 (5–10 mm)	d_3 (10–15 mm)	d_4 (15–20 mm)	d_5 (20–25 mm)
n	0.1	85.13	6.11	3.78	2.77	2.21
	0.3	61.70	14.26	9.83	7.73	6.48
	0.5	44.72	18.52	14.21	11.98	10.56
	0.7	32.41	20.24	17.28	15.60	14.46
	0.9	23.49	20.35	19.31	18.66	18.19
m	0.3	75.97	0	9.83	7.73	6.48
	0.5	54.77	22.69	0	11.98	10.56
	0.7	39.64	24.76	21.14	0	14.46

From Table 1, it can be found that the distribution of the particle size of the broken gangue samples with different Talbot grading indices has great differences. The small particle proportion decreases gradually with the increase in m and n, while that for the large particles is opposite. The particle proportion less than 5 mm decreases with the increase in m and n; however, the size larger than 5 mm exhibits an opposite variation trend. For example, when n increases from 0.1 to 0.9, the proportion of particle size 0–5 mm is reduced by 61.64%, while the proportion for the particle sizes of 5–10, 10–15, 15–20, and 20–25 mm are increased by 14.24, 15.53, 15.89, and 15.98%, respectively. At the same time, it can be found that the proportion of small particles with discontinuous grading is much larger than that of continuous grading, but both have the same proportion of large particles in the test. For example, when the values of m and n are equal and are taken as 0.3, 0.5, and 0.7 mm, the particles of 0–5 mm in discontinuous grading are higher than that of continuous grading by 14.27%, 10.05% and 16.15%, respectively. The particle proportion of different grading samples directly reflects the size of the broken gangue and determines the differences of pore structure. According to the particle size grading in Table 1, five groups of continuous grading samples and three groups of discontinuous grading ones were obtained after combining the filtered gangue particles of different sizes.

2.2. Experimental Setup

The test system consists of a DDL600 electronic universal testing machine (Changchun Mechanical Science Research Institute Co., Ltd., Changchun, China), osmosis device, seepage circuit, hydraulic pump, and hydraulic accessories, as shown in Figure 2. Among them, the seepage circuit consists of a hydraulic pump, pressure sensor, reversing valve, globe valve, flow sensor. The osmotic device is composed of a cylinder, piston, bottom plate, rims, permeable plate. Additionally, the axial force of the DDL600 electronic universal testing machine ranges from 0 to 600 kN, with the measurement accuracy of ±0.5%. The axial displacement measurement ranges from 0 to 80 mm with the accuracy of ±0.5%; the inner diameter of permeation cylinder is 100 mm, with the capacity of 1.57×10^6 mm^3.

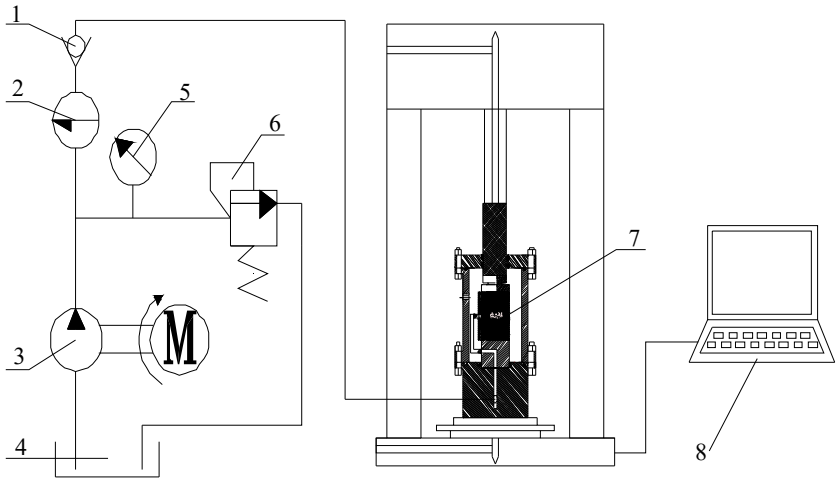

Figure 2. Osmosis system: (1) check valve; (2) flow meter; (3) hydraulic pump; (4) penetrant box; (5) pressure gauge; (6) relief valve; (7) osmosis device; and (8) computer.

Before the experiment, the stability, reliability, and sealing of the entire test system were tested. The osmosis device in the test system is shown in Figure 3. Samples are filled into the osmosis device, and then they are placed on the DDL600 electronic universal testing machine with the upper end contact to the check valve set to 1, and the lower exposure connected to the collecting pail. Before the test, the sample must be saturated in order to fill the piping of the system with osmotic fluid. During the test, the permeate flow rate was obtained by weighing the amount of water infiltrated in the collection tank, and the axial deformation was directly obtained by the test machine data acquisition system.

Figure 3. Filling method of the sample in the osmosis device.

3. Parameter Calculation

3.1. Characteristic Parameters of Compression Deformation

The compression modulus is often used to measure the constrictive strength of broken rock under the condition of lateral restraint, and it describes the change rate of stress relative to the strain, which can be expressed as follows [2]:

$$E_t = \frac{d\sigma_1}{d\varepsilon_1} \tag{2}$$

The differential approximate form of Equation (2) [2] is as follows:

$$E_t = \frac{\Delta\sigma_1}{\Delta\varepsilon_1} \tag{3}$$

The compression of broken rock described by the compression ratio is [2]:

$$\gamma = \frac{\Delta h}{H} \tag{4}$$

where Δh represents the height change of samples at a certain stress level, and H is the initial height of the sample. The compressive rate of broken rock is equal to the value of strain ε in the condition of lateral restraint.

3.2. Permeability Parameter

The porosity of the samples can be calculated by the following Equation (5) [31]:

$$\phi = 1 - \frac{m}{\rho_0 A(h_0 - h_i)} \tag{5}$$

where m is the quality of broken rock, (kg); ρ_0 is the density of sandstone, (kg/m^3); A is the cross-sectional area of broken rock, (m^2); h_0 is the initial height of broken sandstone, (m); and h_i is the height of the sample at the loaded time of t_i for test machine, (m).

The seepage of porous media of broken rock particles is consistent with the relation of Forchheimer [32]:

$$-\frac{\partial p}{\partial h} = \frac{\mu v}{k} + \rho\beta v^2 \tag{6}$$

where p is the osmotic pressure, (MPa); h is the height of the porous medium, (m); ρ is the water density, 1000 kg/m^3; μ is the water viscosity, (Pa·s); v represents the seepage velocity, (m/s); k is the permeability, (m^2); and β is the non-Darcy flow factor, (m^{-1}).

By testing, the time series V_i of cumulative volume of exudate can be obtained, in (t_i,t_{i+1}) time period, the average flow is Q_i, and v_i is the average seepage velocity in (t_i,t_{i+1}) time period:

$$v_i = \frac{Q_i}{A} = \frac{4Q_i}{\pi d^2} \tag{7}$$

where d is the diameter of outlet pipe section.

Since the outlet of penetration connects to the atmosphere, the pressure gradient J at the moment of i is [33]:

$$J = \frac{\Delta P}{h_i} = \frac{P_1 - P_2}{h_i} = \frac{P_1}{h_i} \tag{8}$$

where $\Delta P = P_1 - P_2$ represents the osmotic pressure difference among the samples, and P_1 and P_2 are the pressure in the osmotic inlet and outlet, i.e., $P_2 = 0$. h_i is the height of the sample at the moment of i.

According to Equation (6), the seepage velocity at the moment of i and $i + 1$ is v_i and v_{i+1} respectively, and J is regarded as the pressure gradient. According to the relationship of $v - J$ in i and $i + 1$, the permeability k_i and non-Darcy flow β-factor at time i would be obtained [33]:

$$\begin{cases} J = \frac{\mu v_i}{k} + \rho\beta {v_i}^2 \\ J = \frac{\mu v_{i+1}}{k} + \rho\beta {v_{i+1}}^2 \end{cases} \tag{9}$$

$$\begin{cases} k_i = \frac{\mu v_i v_{i+1}}{J(v_i + v_{i+1})} \\ \beta_i = -\frac{J}{\rho v_i v_{i+1}} \end{cases} \tag{10}$$

4. The Evolution Laws of Deformation and Permeability of Broken Gangue

4.1. The Characteristics of Compression Deformation of Broken Gangue

The samples are given index n values of 0.1, 0.3, 0.5, 0.7, and 0.9 by continuous grading and index m values of 0.3, 0.5 and 0.7 by discontinuous grading with confined compression. The displacement loading method with a loading rate of 0.05 mm/s is applied to all the samples. The relations between stress and strain ($\sigma - \varepsilon$), as well as the relations between the compression modulus and compression ratio ($E_t - \gamma$), of continuous and discontinuous grading samples, are shown in Figure 4. From Figure 4, it can be concluded that the relationships of stress-strain and compression ratio-modulus can all be well fitted by exponential functions under the two different conditions.

As seen from Figure 4a,b, the stress-strain relationship of different continuous-grade samples is approximately the same. With the increase in axial strain, the stress increases exponentially, and the compression modulus is compatible with the increase in the compression ratio. This result means that the greater the compression rate is, the harder it is for the gangue to be compressed. Compared to the stress-strain relationship, it can be observed that, with the decrease in the Talbot exponent, the stress and compressive modulus increase quickly. The smaller the sample's Talbot index is, the more difficult it is to compress. As seen from Figure 4a, with the smaller Talbot index, smaller particles with higher content are filled closely, so the sample is more difficult to compress. Similarly, the relationships of stress-strain and compressive modulus-ratio of the discontinuous grading samples shown in Figure 4c,d are similar to those of the continuous-grade samples, with an increase in stress and strain according to the exponential function. The smaller the discontinuous grading index is, the faster the compression modulus increases with increasing compression rate, i.e., the samples are harder to compress. In addition, there is a great difference in the compression deformation of samples by continuous and discontinuous grading. Taking the samples with index of 0.5 by discontinuous and continuous grading as the examples, when the strain is 0.1, the stress of these samples are 3.35 and 2.76 MPa, respectively, and the compressive modulus are 1.12 and 0.96 MPa; when the strain is 0.25, the stress of the samples is 43.6 and 35.9 MPa, and the compression modulus are 11.8 and 9.6 MPa.

It is indicated that samples with discontinuous grading are more difficult to compress than those with continuous grading, and with an increasing compression rate, the discontinuous grading samples are denser, because the particles are also denser in arrangement.

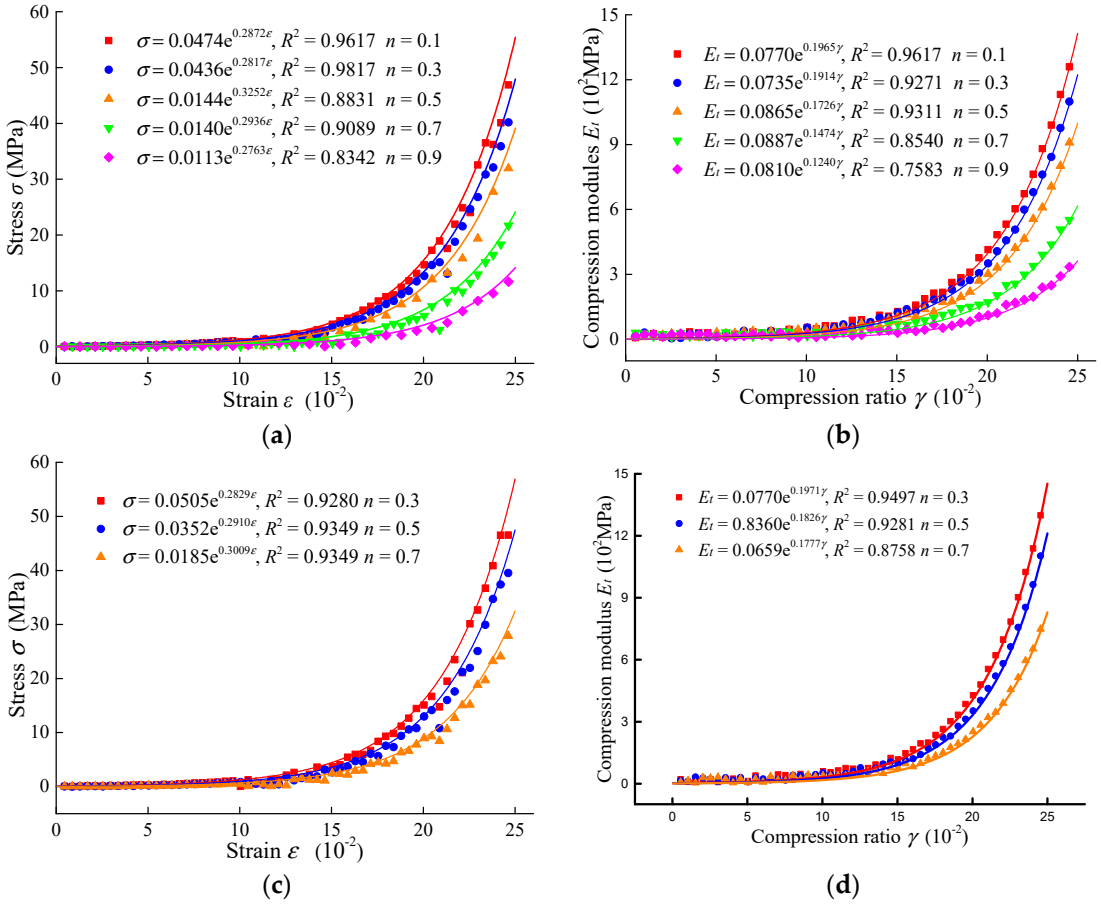

Figure 4. The compression properties of broken gangue: (**a**) relationship of stress-strain by continuous grading; (**b**) relationship of compression modulus-ratio by continuous grading; (**c**) relationship of stress-strain by discontinuous grading; and (**d**) the relationship of the compression modulus-ratio by discontinuous grading.

4.2. The Evolution Characteristics of Permeability of Grading Broken Gangue

To study the permeability of broken rock in the whole process of compression, the permeability parameters of grading broken gangue were tested. At the same time, the change law of exudate is recorded with the change in the compression rate. To reduce the influence of osmotic pressure on the compression process, the osmotic pressure was fixed at 2 MPa. The change law of the total flow rate and seepage velocity of exudate with the compression rate under different grading conditions are shown in Figure 5a,b. In addition, the permeability and non-Darcy flow β-factor variation trends with the compression rate are shown in Figure 5c,d, respectively (note: Figure 5b can be obtained by Equation (7), and Figure 5c,d can be obtained by Equation (10)).

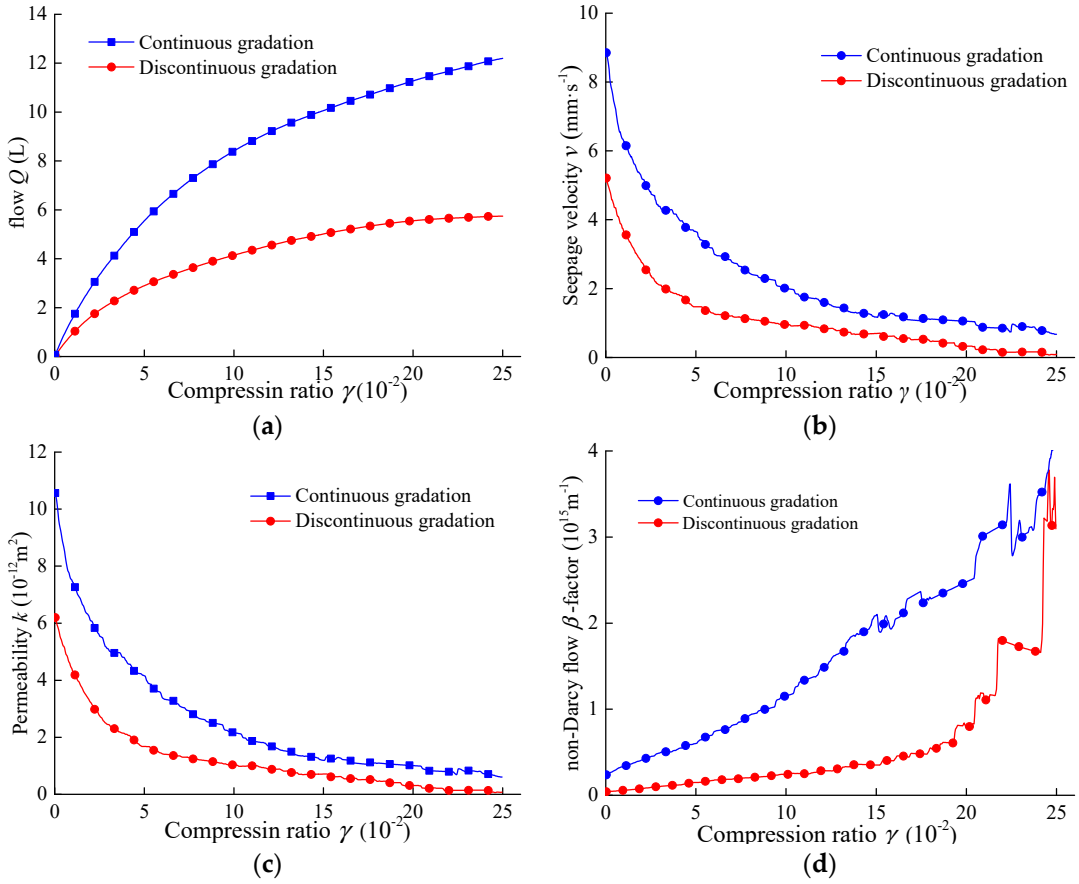

Figure 5. Evolution law of seepage characteristic of broken gangue under compression condition: (**a**) evolution law of cumulative flow; (**b**) evolution law of seepage velocity; (**c**) evolution law of permeability; and (**d**) evolution law of β-factor for non-Darcy flow.

As seen from Figure 5, the evolution law of permeability of broken gangue by discontinuous and continuous grading under axial loading conditions is basically the same. The cumulative flow and non-Darcy flow β-factor show a nonlinear increasing trend with increasing compression rate, but with an increasing rate contrary to the above situation. With increasing compression rate, the seepage velocity and permeability are characterized by decreasing nonlinearly. In addition, there are obvious differences in the evolution law of permeability for discontinuous and continuous grading. Compared with continuous-grade broken gangue, the increased rate of cumulative flow of the discontinuous-grade samples is smaller under the same compression rate, and the cumulative flow is also smaller. With an increasing compression rate, the seepage velocity and permeability of discontinuous and continuous grading of broken gangue gradually decrease, with a nonlinear decreasing trend for the decreasing rate; and the seepage velocity and permeability of the discontinuous grading sample are smaller at initial values, that the decrease rate is faster and that the final value is smaller. With the increasing compression rate, the non-Darcy flow β-factor shows a linear increasing trend by continuous grading, which is the opposite of the discontinuous grading samples. However, the final non-Darcy flow β-factor of these samples was similar.

From Figure 4, broken gangue was denser and less compressible with a high compression rate. Therefore, the variation range of cumulative flow, seepage velocity, and permeability all decrease with the increasing compression rate while, for a higher compression rate of broken gangue, the pore is smaller and fluid resistance is greater, which contributes heavily to nonlinear seepage; as a result, the non-Darcy flow β-factor is larger.

As seen from Figure 5, the smaller particle size of broken gangue under discontinuous grading occupies a higher proportion of space; the pores between large particles are easily filled; and mixed

samples are denser, so the seepage velocity and permeability are small in the initial state. The pores are filled densely with small particles. Thus, the samples are more difficult to compress, and the decreasing speed of permeability becomes steadily smaller under a high compression rate.

4.3. Influence of Stress on the Permeability of Grading Broken Rock

The above study shows that compressibility and permeability of broken gangue depends on the compression state, while the compressive state of the broken gangue is related to axial stress. To study the relationship between axial stress and permeability of broken rock, the axial stress of 5 MPa is used to compress grading broken gangue first. Then, after fixing the load displacement and testing permeability parameter of broken gangue under the present conditions by a steady-state method, the permeability tests under 10, 15, 20, 25, and 30 MPa are completed. Finally, the permeability tests of broken gangue samples were completed in the same way with continuous and discontinuous grading.

In Figure 6, the permeability of broken gangue under different compressive stress is displayed. It can be seen from the graph that the permeability of broken gangue shows a negative exponential function, decreasing with the increase in axial compressive stress. The permeability decreases rapidly when the compressive stress is less than 15 MPa; when the compressive stress is more than 15 MPa, the permeability decreases gently. This result shows that axial compression has significance in reducing the permeability of broken gangue when the compressive stress is less than 15 MPa; however, when the compressive stress is greater than 15 MPa, the effect is not obvious.

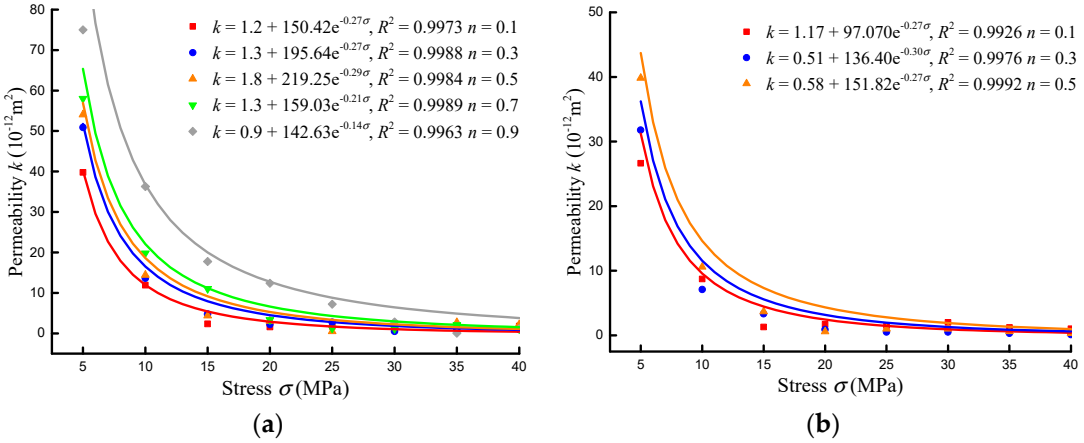

Figure 6. Permeability of broken gangue with different compressive stress: (**a**) continuous grading; and (**b**) discontinuous grading.

Second, under the same stress, the larger the grading index, the higher the permeability of broken gangue is, and the more significant the axial compression is to reduce the permeability of the sample. For example, for continuous grading samples, when the stress increases from 5 MPa to 40 MPa, the permeability of n = 0.9 decreases from 76 to 7 μm^2; for n = 0.1, the permeability decreases from 39 to 4 μm^2; and the change amplitudes is 69 and 35 μm^2, respectively.

In addition, the axial stress of discontinuous grading gangue must be smaller in order to achieve the same permeability level. For n = 0.5, axial stress of continuous grading should be set to 10 MPa, and that for discontinuous grading should be set at 8 MPa to make the permeability of samples reduce to 20 μm^2; in continuous grading, the data should be 15 MPa, while with discontinuous grading requiring 12 MPa to make the permeability of samples reduce to 10 μm^2.

It can be found that, for grading broken gangue, with a higher proportion of small particles, the particles are easier to adjust by sliding and rolling due to axial stress in order to achieve a tighter state. However, in the process of compression, samples with many large particle sizes must overcome the dislocation of large particles. Therefore, it is more difficult to compress them.

These conclusions are quite consistent with previous research by Harianto Rahardjo [34]. In the mixed gangue particle samples, the pores generated by accumulation of large particles are usually occupied by small particles, which result in the higher compressibility of discontinuous grading samples. Therefore, considering the permeability-mechanical response, appropriate backfill material properties need to be considered in the application of gangue filling mining project. After the coal has been mined, the backfill material plays the supporting role of the roof rock mass, which is a critical concern for controlling surface subsidence [12].

5. Conclusions

The broken rock mass is widely distributed in underground engineering, and it is very important to the stability of these engineering, especially, the deformation characteristic and permeability could be the pivotal factor in the migration of underground water. The deformation and permeability of broken gangue as a function of the stress level and grading features were studied through confined compression and pressed seepage tests. This research indicates that with the increase in axial strain, the stress of broken gangue increases with an exponential function, and the compression modulus is increased with increasing compression ratio, which indicates that the greater compression rate of broken gangue is, the harder it is to be compressed. Samples by discontinuous grading are harder to compress than those of continuous grading, and the former is denser with the increase in compression rate. Discontinuous grading has a larger number of small particle components and a denser grain arrangement based on both tests. Therefore, samples by discontinuous grading are more difficult to compress. With increasing compression rate, the change range of seepage velocity and permeability of broken gangue decreases, with a higher compression rate of broken gangue and smaller pores, the fluid has higher resistance. All these factors lead to stronger nonlinear characteristics of seepage, the larger the grading index of broken gangue is, the more remarkable effect of axial compression on reducing the permeability of the samples. To achieve the same permeability level, compared to that of continuous grading, the axial stress by the discontinuous grading sample is smaller. Finally, through the research and discussion in this paper, the mixed gangue particle samples with smaller grading index are more suitable for backfill material, and the performance of discontinuous grading samples is better in resistance of compression and penetration. Therefore, the broken gangue with discontinuous grading and small grading index is more suitable as filling material, meanwhile fault fractured zones and the collapse columns with the same characteristics are less prone to water inrush accidents.

Author Contributions: Y.Z. contributed to the experimental design and sourcing of the laboratory equipment and raw materials; W.Z. carried out the permeability analysis of grading broken gangue; M.L. contributed to the experimental operation, data collection, and writing of the manuscript; and Z.C. also contributed in the experimental design and correction of the manuscript.

Funding: This paper was support by the National Key Research and Development Plan (2016YFC0501103), National Natural Science Foundation of China (51574222, 51704281).

Acknowledgments: The authors gratefully acknowledge Qiang Li, who has given us many useful ideas and suggestions.

Conflicts of Interest: The authors declare no conflict of interest.

References

1. Manouchehrian, A.; Cai, M. Numerical modeling of rockburst near fault zones in deep tunnels. *Tunn. Undergr. Space Technol.* **2018**, *80*, 164–180. [CrossRef]
2. Yin, Q.; Jing, H.W.; Su, H.J.; Zhao, H.H. Experimental study on mechanical properties and anchorage performances of rock mass in the fault fracture zone. *Int. J. Geomech.* **2018**, *18*, 04018067. [CrossRef]
3. Zheng, Y.L.; Zhang, Q.B.; Zhao, J. Challenges and opportunities of using tunnel boring machines in mining. *Tunn. Undergr. Space Technol.* **2016**, *57*, 287–299. [CrossRef]
4. Sparks, R.S.J.; Wilson, L.; Hulme, G. Theoretical modeling of the generation, movement, and emplacement of pyroclastic flows by column collapse. *J. Geophys. Res. Solid Earth* **1978**, *83*, 1727–1739. [CrossRef]

5. Sparks, R.S.J. A model for the formation of ignimbrite by gravitational column collapse. *J. Geol. Soc. Lond.* **1976**, *132*, 441–451. [CrossRef]
6. Utili, S.; Zhao, T.; Houlsby, G.T. 3D DEM investigation of granular column collapse: Evaluation of debris motion and its destructive power. *Eng. Geol.* **2015**, *186*, 3–16. [CrossRef]
7. Huang, Y.; Li, J.; Song, T.; Kong, G.; Li, M. Analysis on Filling Ratio and Shield Supporting Pressure for Overburden Movement Control in Coal Mining with Compacted Backfilling. *Energies* **2016**, *10*, 31. [CrossRef]
8. Ma, C.Q.; Li, H.; Zhang, P. Subsidence prediction method of solid backfilling mining with different filling ratios under thick unconsolidated layers. *Arab. J. Geosci.* **2017**, *10*, 511. [CrossRef]
9. Zhang, L.T. Summary on the dam-break of tailing pond. *J. Hydraul. Eng. ASCE* **2013**, *44*, 594–600.
10. Wang, F.T.; Zhang, C.; Wei, S.F.; Zhang, X.G.; Guo, S.H. Whole section anchor–grouting reinforcement technology and its application in underground roadways with loose and fractured surrounding rock. *Tunn. Undergr. Space Technol.* **2016**, *51*, 133–143.
11. Wu, X.Z.; Jiang, Y.J.; Guan, Z.C.; Wang, G. Estimating the support effect of energy-absorbing rock bolts based on the mechanical work transfer ability. *Int. J. Rock Mech. Min. Sci.* **2018**, *103*, 168–178. [CrossRef]
12. Cao, W.H.; Wang, X.F.; Li, P.; Zhang, D.S.; Sun, C.D.; Qin, D.D. Wide Strip Backfill Mining for Surface Subsidence Control and Its Application in Critical Mining Conditions of a Coal Mine. *Sustainability* **2018**, *10*, 700. [CrossRef]
13. Li, J.; Huang, Y.; Qiao, M.; Chen, Z.; Song, T.; Kong, G.; Gao, H.; Guo, L. Effects of Water Soaked Height on the Deformation and Crushing Characteristics of Loose Gangue Backfill Material in Solid Backfill Coal Mining. *Processes* **2018**, *6*, 64. [CrossRef]
14. Cai, W.; Dou, L.M.; Li, Z.L.; He, J.; He, H.; Ding, Y.L. Mechanical Initiation and Propagation Mechanism of a Thrust Fault: A Case Study of the Yima Section of the Xiashi-Yima Thrust (North Side of the Eastern Qinling Orogen, China). *Rock Mech. Rock Eng.* **2015**, *48*, 1–19. [CrossRef]
15. Nakashima, S.; Kishida, K.; Adachi, T.; Izu, Y. Experimental Study on the Stability of Dam Foundation in Consideration of the Effect of the Concrete Plug Treatments. *Fish. Sci.* **2000**, *66*, 915–923.
16. Dong, H.; Hu, Z.R.; Fu, H.L.; Chen, C.; Chen, X.W. Analysis of deformation characteristics of eluvial gravel soil under mass density and confining pressure. *J. Cent. South Univ.* **2015**, *46*, 3879–3887. [CrossRef]
17. Yin, Z.Q.; Li, X.B.; Jin, J.F.; He, X.-Q.; Du, K. Failure characteristics of high stress rock induced by impact disturbance under confining pressure unloading. *Trans. Nonferrous Met. Soc. China* **2012**, *22*, 175–184. [CrossRef]
18. Scheingross, J.S.; Minchew, B.M.; Mackey, B.H.; Simons, M.; Lamb, M.P.; Hensley, S. Fault-zone controls on the spatial distribution of slow-moving landslides. *Geol. Soc. Am. Bull.* **2013**, *125*, 473–489. [CrossRef]
19. Li, H.; Bai, H.B.; Wu, J.J.; Ma, Z.; Ma, K.; Wu, G.; Du, Y.; He, S. A Cascade Disaster Caused by Geological and Coupled Hydro-Mechanical Factors—Water Inrush Mechanism from Karst Collapse Column under Confining Pressure. *Energies* **2017**, *10*, 1938. [CrossRef]
20. Yin, Q.; Jing, H.W.; Ma, G.W.; Su, H.; Liu, R. Investigating the roles of included angle and loading condition on the critical hydraulic gradient of real rock fracture networks. *Rock Mech. Rock Eng.* **2018**, *51*, 3167–3177. [CrossRef]
21. Mudd, G.M. Critical review of acid in situ leach uranium mining: 1. USA and Australia. *Environ. Geol.* **2001**, *41*, 390–403. [CrossRef]
22. Chai, J.R. Analysis of nonlinear seepage through fracture network in rock mass. *J. Hydrodyn.* **2002**, *17*, 217–221.
23. Min, K.B.; Rutqvist, J.; Tsang, C.F.; Jing, L. Stress-dependent permeability of fractured rock masses: A numerical study. *Int. J. Rock Mech. Min. Sci.* **2004**, *41*, 1191–1210. [CrossRef]
24. Noiriel, C.; Gouze, P.; Bernard, D. Investigation of porosity and permeability effects from microstructure changes during limestone dissolution. *Geophys. Res. Lett.* **2004**, *31*, 1183–1186. [CrossRef]
25. Liu, M.; Shabaninejad, M.; Mostaghimi, P. Predictions of permeability, surface area and average dissolution rate during reactive transport in multi-mineral rocks. *J. Pet. Sci. Eng.* **2018**, *170*, 130–138. [CrossRef]
26. Moosavi, S.A.; Goshtasbi, K.; Kazemzadeh, E.; Bakhtiari, H.A.; Esfahani, M.R.; Vali, J. Relationship between porosity and permeability with stress using pore volume compressibility characteristic of reservoir rocks. *Arab. J. Geosci.* **2014**, *7*, 231–239. [CrossRef]
27. Tang, Z.; Dong, X.; Yang, Y.; Ma, L. Research on the relationship between grain composition and repose angle of coal gangue in Dongkuang mine, Heshan city, Guangxi, China. *J. Earth Sci.* **2014**, *25*, 309–314. [CrossRef]

28. Hunter, R.P.; Bowman, E.T. Visualisation of seepage induced suffusion and suffosion within internally erodible granular media. *Geotechnique* **2017**, *68*, 918–930. [CrossRef]
29. Bush, R.T. A theory of particle interference based upon the uncertainty principle. *Lettere al Nuovo Cimento* **1983**, *36*, 241–244. [CrossRef]
30. Miao, X.X.; Li, S.C.; Liu, W.Q. Experimental Study of Seepage Properties of Broken Sandstone under Different Porosities. *Transp. Porous Media* **2011**, *86*, 805–814. [CrossRef]
31. Zhou, J.Q.; Hu, S.H.; Fang, S.; Chen, Y.F.; Zhou, C.B. Nonlinear flow behavior at low Reynolds numbers through rough-walled fractures subjected to normal compressive loading. *Int. J. Rock Mech. Min. Sci.* **2015**, *80*, 202–218. [CrossRef]
32. Meraj, M.A.; Shehzad, S.A.; Hayat, T.; Abbasi, F.M.; Alsaedi, A. Darcy-Forchheimer flow of variable conductivity Jeffrey liquid with Cattaneo-Christov heat flux theory. *Appl. Math. Mech.* **2017**, *38*, 557–566. [CrossRef]
33. Yin, Q.; Ma, G.W.; Jing, H.W.; Wang, H.; Su, H.; Wang, Y.; Liu, R. Hydraulic properties of 3D rough-walled fractures during shearing: An experimental study. *J. Hydrol.* **2017**, *555*, 169–184. [CrossRef]
34. Rahardjo, H.; Satyanaga, A.; D'Amore, G.A.R.; Leong, E.-C. Soil–water characteristic curves of gap-graded soils. *Eng. Geol.* **2012**, *125*, 102–107. [CrossRef]